Photothermal Radiometry with Solid Cylindrical Samples

Chinhua Wang, Andreas Mandelis, and Yue Liu
Center for Advanced Diffusion Wave Technologies, Department of Mechanical and Industrial Engineering, University of Toronto, M5S 3G8 Canada

(Received 16 February 2004; accepted 14 June 2004)

We extend the applications of the photothermal diagnostics by means of laser-infrared photothermal radiometry (PTR) to samples with curved surfaces. Specifically, we present both the theoretical and experimental PTR studies on solid cylindrical samples (surfaces). Based on the Green function method, the thermal-wave field distribution of a cylindrical surface that is under the excitation of a periodically modulated uniform beam is obtained. The laser beam, which is of a cylindrical symmetry, impinges uniformly, partially or fully, on the cylindrical surface, which is practically infinitely long along the axial direction. The characteristics of the thermal-wave field with respect to the thermal diffusivity of the material, the diameter of the sample, the size of the incident beam, and the measurement of the angle are discussed. Experimental results are in good agreement with the theory. © *2004 American Institute of Physics*. [DOI: 10.1063/1.1779973]

I. INTRODUCTION

Since the emergence of the photothermal radiometry (PTR) technique in the early 1980s, it has become a very powerful tool for the thermal characterization and the nondestructive evaluation of broad classes of materials.[1–4] The basic principle of PTR is the measurement of changes in the thermal- (infrared-) radiation emission from a material as a result of the absorption of an intensity-modulated laser beam, which can be quantitatively evaluated by the Stefan-Boltzmann law based on the laser-induced oscillating temperature distribution in the sample. However, all the studies of the PTR technique so far have been mainly focused on flat-surface samples, for which either a one-dimensional (1D)[3] or a three-dimensional[4,5] theoretical model has been developed and applied in various material studies depending on the relative size of the incident-beam spot size and the thermal-diffusion length within the modulation frequency range of interest. Recently, applications of PTR have been extended to the quantitative evaluation of cylindrical and spherical subsurface structures representing the different classes of defects or inclusions.[6–8] Although the PTR signal is generated as a result of the interaction of the thermal waves and the subsurface cylindrical or spherical structures in this type of inhomogeneous material, nevertheless, the measurement of the PTR signal is the same as that in the homogeneous samples in the sense that the thermal radiation is still emitted from a flat surface. An experimental effort has been made to measure the dc temperature of metallic fine wires (~130 μm in diameter) using the PTR technique.[9] The temperature of the wires was measured from the ratio of the photothermal emission signals at two wavelengths. Such ratios of the PTR signals at two wavelengths, however, normalize out the ac part of the temperature, which is induced by the excitation laser beam, and thus, besides the dc temperature value, they cannot provide any useful information about the thermophysical properties of the material.

In this paper, we extend the applications and the measurements of the thermophysical properties of PTR to the samples with curved surfaces. Specifically, we present both the theoretical and the experimental PTR studies on solid cylindrical samples (surfaces). Based on the Green function method,[10] the temperature-field distribution of a cylindrical surface under the excitation of a periodically modulated uniform beam is obtained. The characteristics of the temperature field related to the different measurement parameters are discussed, and finally, the theoretical model is further validated experimentally with cylindrical steel samples of different diameters.

II. THEORY

The thermal-wave field in a cylindrical sample of radius R_0 and of infinite length, which is induced by a modulated optical excitation of the cylindrical (curved) surface, can be derived based on the Green function method. The geometry and the coordinates of the boundary-value problem are shown in Fig. 1.

The exciting laser beam, which is of a cylindrical symmetry and subtends at an angle θ_0, impinges uniformly on the cylindrical surface, which is assumed to be infinitely long along the axial direction in conformity with typical experimental geometries. Considering the harmonic modulation of

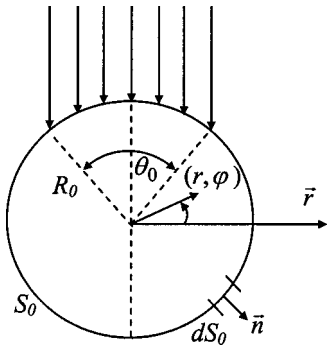

FIG. 1. Cross-sectional geometry of an infinite-height cylinder of radius R_0 externally excited photothermally by a uniform light beam impinging on part of its surface subtending a sector of an angle θ_0.

the incident exciting light, the governing thermal-wave equation for the material under investigation can be written as

$$\nabla^2 T(\vec{r},\omega) - \sigma^2(\omega) T(\vec{r},\omega) = -\frac{1}{k} Q(\vec{r},\omega), \tag{1}$$

where $\sigma(\omega) = (i\omega/\alpha)^{1/2} = (1+i)\sqrt{\omega/2\alpha}$ is the thermal wave number, $\alpha(\mathrm{m}^2/\mathrm{s})$ and k (W/K m) are, respectively, the thermal diffusivity and the thermal conductivity of the material, ω is the angular modulation frequency, and $Q(\vec{r},\omega)$ is the volume thermal source at coordinates (r,φ) inside the material. Based on the Green function method, the general solution for Eq. (1) can be expressed as[10]

$$\begin{aligned} T(r,\omega) = (\alpha/k) &\int\int\int_{V_0} Q(\vec{r}_0,\omega) G(\vec{r}|\vec{r}_0;\omega) dV_0 \\ &+ \alpha \oint_{S_0} [G(\vec{r}|\vec{r}\,^s_0;\omega) \nabla_0 T(\vec{r}\,^s_0;\omega) \\ &- T(\vec{r}\,^s_0,\omega) \nabla_0 G(\vec{r}|\vec{r}\,^s_0;\omega)] \cdot d\vec{S}_0, \end{aligned} \tag{2}$$

where S_0 is the surface surrounding the domain volume V_0, which includes the harmonic source $Q(\vec{r}_0,\omega)$, $\vec{r}\,^s_0$ is the source coordinate point on surface S_0, $d\vec{S}_0$ indicates an infinitesimal area vector along the outward direction normal to the boundary surface S_0: $d\vec{S}_0 = \vec{n} dS_0$ with $\vec{n}$ being the outward unit vector, as shown in Fig. 1, and $G(\vec{r}|\vec{r}_0;\omega)$ is the Green function (units: $\mathrm{s/m}^3$) that satisfies the equation $\nabla^2 G(\vec{r},\omega) - \sigma^2(\omega) G(\vec{r},\omega) = -\delta(\vec{r}-\vec{r}_0)/\alpha$ in the case of a periodic heat source. The physical interpretation of the thermal-wave Green function is that it represents the temperature modulation anywhere in a given domain due to a harmonic heat source of a unit strength located at point $\vec{r} = \vec{r}_0$ within the domain and represented by the Dirac delta function $\delta(\vec{r} - \vec{r}_0)$.[10–12] The Green function $G(\vec{r}|\vec{r}_0;\omega)$ takes different forms depending on the types of boundary conditions, e.g., Dirichlet, Neumann, mixed (third kind), and imposed on the investigated material.

In the most general case, when a laser beam is incident onto a homogeneous solid material that is not entirely opaque, the material will absorb some of the photon energy and thus generate a volume heat source inside the material. Depending on the surface conditions of the material, different types of the boundary conditions may apply. Therefore, the temperature field must be evaluated using the complete form of Eq. (2). However, in most cases, Eq. (2) can be simplified depending on specific material properties. For solids with high attenuation of the incident light, such as metallic samples, the absorption of the incident light occurs at the surface, and therefore, the volume source can be neglected. In this paper, we will focus on opaque materials. In this case, the boundary conditions upon the incidence of an expanded uniform laser beam can be written as

$$k \frac{\partial}{\partial n} T(r,\varphi,\omega)\bigg|_{r=R_0} = F(R_0,\varphi,\omega), \tag{3}$$

with $F(R_0,\varphi,\omega)$ being the incident thermal flux on the cylinder surface. It should be mentioned that the convection-heat-transfer term $h(T-T_\infty)$ between the material and the ambient medium (air) is neglected, where h is the heat-transfer coefficient, and T and T_∞ are the temperatures of the material and the ambient, respectively. This can be justified by the small heat-transfer coefficient $h(\sim 0.1\ \mathrm{W/m^2\ K})$ between the material and the static air[12] and the small temperature difference between the sample and the ambient medium ($\ll 1$ K) when compared with the incident heat flux $F(R_0,\varphi,\omega)$ ($\sim 10^5\ \mathrm{W/m^2}$ for 1 W laser beam with a 10 mm^2 spot size). Neglecting the convection-heat-transfer term can also be justified by the very small (~ 0.1 in our case) Grashof number (Gr number); free convection is effectively suppressed when the Gr number is below 2000.[13] Assuming that the incident light on the surface is uniform, in conformity with our PTR system, the thermal flux must be weighed by a projection factor in the form of the cosine of the incident uniform light intensity and can be expressed as

$$F(R_0,\varphi,\omega) = F_0 \begin{Bmatrix} \cos(\pi/2-\varphi); (\pi-\theta_0)/2 \leqslant \varphi \leqslant (\pi+\theta_0)/2 \\ 0;\ \text{all other angles} \end{Bmatrix}. \tag{4}$$

The appropriate Green function corresponding to the foregoing boundary condition is[10]

$$G(r,\varphi|r_0,\varphi_0;\omega) = \frac{1}{2\pi\alpha} \sum_{m=-\infty}^{\infty} \frac{e^{im(\varphi-\varphi_0)}}{I'_m(\sigma R_0)} \times \begin{Bmatrix} [I'_m(\sigma R_0) K_m(\sigma r_0) - I_m(\sigma r_0) K'_m(\sigma R_0)] I_m(\sigma r), & 0 \leqslant r \leqslant r_0 \\ [I'_m(\sigma R_0) K_m(\sigma r) - I_m(\sigma r) K'_m(\sigma R_0)] I_m(\sigma r_0), & r_0 \leqslant r \leqslant R_0 \end{Bmatrix} \tag{5}$$

with derivatives of the modified Bessel functions of the first and second kind, I_m and K_m

$$I'_m(\sigma R_0) \equiv \frac{d}{dr} I_m(\sigma r)\bigg|_{r=R_0} = \sigma I_{m-1}(\sigma R_0) - \frac{m}{R_0} I_m(\sigma R_0), \tag{6}$$

and

$$K'_m(\sigma R_0) \equiv \frac{d}{dr} K_m(\sigma r)\bigg|_{r=R_0} = -\sigma K_{m-1}(\sigma R_0) - \frac{m}{R_0} K_m(\sigma R_0). \tag{7}$$

Since $\vec{n} \cdot \nabla G|_{r=R_0} = 0$, and in the absence of volume sources, the field equation [Eq. (2)] becomes

$$T(r,\varphi,\omega)=\alpha\oint_{S_0} G\left(\vec{r}|\vec{r}\,^{S}_{0};\omega\right)\nabla_0 T(\vec{r}\,^{S}_{0},\omega)\cdot d\vec{S}_0$$
$$=\frac{R_0\alpha F_0}{k}\int_{\pi/2-\theta_0/2}^{\pi/2+\theta_0/2} G(\vec{r}|\vec{r}\,^{S_0}_{0};\omega)\cos(\pi/2-\varphi_0)d\varphi_0. \tag{8}$$

Substituting the Green function into Eq. (6), interchanging $(r,\varphi)\Leftrightarrow(r_0,\varphi_0)$ so as to allow integration over the source coordinates (r_0,φ_0), and using the identities

$$\sum_{m=-\infty}^{\infty} e^{im(\varphi-\varphi_0)}=1+2\sum_{m=1}^{\infty}\cos[m(\varphi-\varphi_0)], \tag{9}$$

and

$$I_m(x)=I_{-m}(x), \tag{10}$$

the resulting thermal-wave field can be finally expressed as

$$T(r,\varphi,\omega)=\frac{F_0}{2\pi k}\left\{\frac{2I_0(\sigma r)}{I_0'(\sigma R_0)}\sin\frac{\theta_0}{2}+\frac{I_1(\sigma r)}{I_1'(\sigma R_0)}(\theta_0+\sin\theta_0)\right.$$
$$\times\cos\left(\frac{\pi}{2}-\varphi\right)+2\sum_{m=2}^{\infty}\frac{I_m(\sigma r)}{I_m'(\sigma R_0)}$$
$$\times\cos\left[\frac{m}{2}(\pi-2\varphi)\right]\left[\frac{\sin[(m+1)\theta_0/2]}{m+1}\right.$$
$$\left.\left.+\frac{\sin[(m-1)\theta_0/2]}{m-1}\right]\right\}. \tag{11}$$

In order to simplify the resulting expression, the Wronskian formula[14]

$$K_m(\sigma R_0)\left[\frac{d}{dr}I_m(\sigma r)\bigg|_{r=R_0}\right]-I_m(\sigma R_0)$$
$$\times\left[\frac{d}{dr}K_m(\sigma r)\bigg|_{r=R_0}\right]=\frac{1}{R_0} \tag{12}$$

was employed.

Equation (11) gives the thermal-wave field at any point inside the cylindrical sample. From the structure of this expression, it is seen that the frequency dependence of the thermal-wave field of the cylindrical samples under the illumination of a uniform light beam is a strong function of the material thermal diffusivity.

III. NUMERICAL CALCULATIONS

Although Eq. (11) explicitly demonstrates the relationship between the temperature field and the thermophysical parameters, as well as several geometric and measurement configuration factors for a cylindrical sample, the complicated functional dependence of the signal on the various system parameters makes any attempt for further understanding of the system behavior under a photothermal probe difficult. To gain more physical insights into the characteristics of the ac temperature field, it is instructive to study its dependence on each individual parameter involved in Eq. (11). Considering the measurement nature of the PTR technique, only the thermal-wave field on the sample surface $(r=R_0)$ will be evaluated in the following simulations. In all simulations, the amplitude and the phase of the surface-temperature oscillation are normalized to the corresponding amplitude and phase of a flat surface of a semi-infinitely thick sample of the same material in order to see the effects of the curved surface with an optimal contrast. The amplitude and the phase of a flat surface are calculated based on the well-known 1D theoretical model, which is valid under the condition that the incident-beam size is much larger than the thermal-diffusion length of the material within modulation frequency range of interest. Under illumination with a constant thermal flux F_0 at the surface of the flat sample, the temperature field evaluated at the surface is given by[10]

$$T(0,\omega)=F_0\left(\frac{\sqrt{\alpha}}{k\sqrt{\omega}}\right)e^{-i\pi/4}, \tag{13}$$

where α and k are the thermal diffusivity and the thermal conductivity of the material, respectively. The thermal-wave field given in Eq. (13) clearly exhibits the well-known dependence of the amplitude on the inverse of the square root of the frequency and a constant $(\pi/4)$ phase lag of the temperature oscillation with respect to the incident thermal flux.

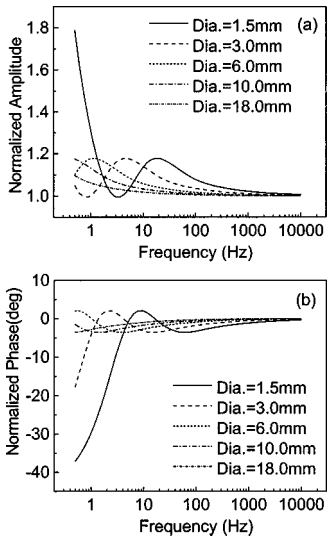

FIG. 2. Effect of the diameter of the cylindrical sample on the thermal-wave field measured at the sample surface $(r=R_0)$ and at the angle $\varphi=90°$. The amplitude and the phase are normalized, respectively, to the corresponding values of a flat surface of the same material.

Figure 2 shows the effect of the diameter of the cylindrical sample on the thermal-wave field measured at the sample surface $(r=R_0)$ and at an angle of $\varphi=90°$. The beam size is assumed to be large enough so as to cover the entire upper part of the cylinder; therefore, $\theta_0=180°$ is assumed in the calculation. The other material parameters used in the simulation are as follows: $\alpha=13.57\times10^{-6}$ m^2/s for AISI 1018 carbon steels,[15] $F_0=1$ W/cm^2, and $k=51.9$ W/K m.

It is seen that, as the diameter of the cylinder increases, both the normalized amplitude and phase curves become flatter, an indication that the thermal-wave field from thicker cylinders reduces gradually to that of a flat surface, as expected. It is also shown that, at the high-frequency end, both

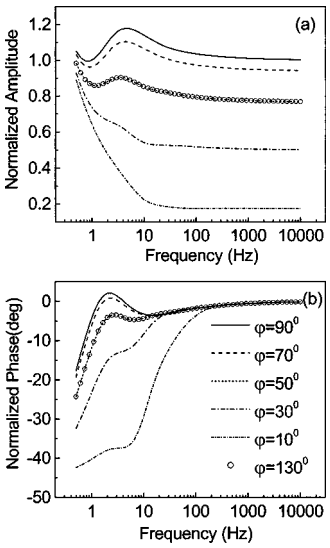

FIG. 3. Normalized surface ($r=R_0$) thermal-wave amplitude and phase at various measurement angles for a cylinder with a diameter of 3.0 mm. Both plots have the same symbol notations for different angles.

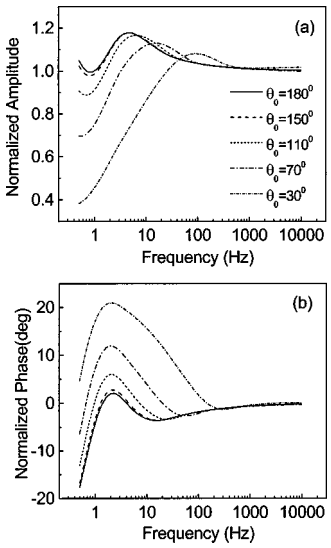

FIG. 4. Normalized surface (measured at $r=R_0$ and $\varphi=90°$) thermal-wave amplitude and phase with different laser-beam sizes subtending at different angles θ_0, Fig. 1, for a cylinder with a diameter of 3.0 mm. Both plots have the same symbol notations for different angles.

the amplitude and the phase converge toward the corresponding value of the flat surface. This can be explained by the shorter thermal-diffusion length at higher modulation frequencies: The curved thin slice of the cylinder contained within a thermal-diffusion length below the surface can be approximated by a flat surface at higher frequencies with an increasing degree of accuracy. Therefore, the relatively smaller thermal-diffusion length at the higher frequencies, compared to the surface curvature, resembles more closely a thermal-wave propagation in a flat material (zero surface curvature). Conversely, the highest degree of sensitivity of the thermal-wave field to the curvature occurs when the thermal-diffusion length is commensurate with the curvature. The physical origin of the oscillating peaks observed in both the amplitude and the phase can be understood by the thermal-wave interference within the bulk of the cylinder under accumulation boundary conditions[10,16] similar to those observed in a flat sample with a finite thickness.[17] Here, the boundary of the finite-diameter cylinder confines the thermal waves and forms a low-Q resonant cavity,[18] as witnessed by the stronger interference effect in the smaller diameter cylinders. This effect gradually decays due to the highly damped nature of the thermal waves, as the diameter increases to a certain limiting value at which point it is considered infinite.

Figure 3 shows the angular effect of the thermal-wave field vs the modulation frequency on the cylindrical surface (diameter=3.0 mm) when the illumination of the incident beam is expanded to cover the whole upper part of the cylinder (i.e., $\theta_0=\pi$), and also large enough to be described by a 1D model in the limit of a flat surface to which the field under the curvature is normalized.

Although uniform illumination is applied on the half surface, the thermal flux is not uniform due to the projectional nature of the incident flux, $-k\vec{n}\cdot\nabla_0 T(\vec{r}_0^{\,s};\omega)$, on the cylindrical surface. As a result, at a fixed frequency, the thermal-wave distribution on the sample surface over the angular coordinates becomes bell shaped, with peak value near 90°, and flanked by two symmetrical wings at coordinates near 0° or 180°. At different angles, the frequency scans show different behaviors in both the amplitude and the phase. The field near 90° exhibits stronger thermal-wave interference than that near 0° or 180°. This is probably due to the weaker confinement of the thermal-wave field determined by the larger tangential angle formed by the upper and lower cylindrical surfaces at positions near 0° or 180°. At $\varphi=0°$ or 180°, the formation of a thermal standing wave is not possible at the given frequency due to the maximum effective thickness of the cavity formed by the upper and lower sectors of the cylindrical surface along the axis of symmetry at 90°. Due to the symmetry of illumination about the 90 degree axis perpendicular to the surface, the thermal-wave field also exhibits its symmetry, as can be seen from the coincidence of the two-frequency scan curves at $\varphi=50°$ and 130°, as expected. In conclusion, thermal-wave interference within the cylindrical cavity appears to be most strongly observable at an angle of $\varphi=90°$ along the direction of irradiation.

Figure 4 shows the effect of laser-beam size on the thermal-wave field when measured at $\varphi=90°$ for a steel sample with a diameter of 3.0 mm. The normalization is still performed with the temperature field of a 1D flat solid with the same thermophysical properties. As expected, the amplitude peak decreases at smaller angles θ_0 due to the decreased thermal-wave flux into the solid, and it shifts to higher frequencies as the effective distance to the solid-air boundary decreases with more of the (nonilluminated sideways) curved surface contributing to the confinement of the thermal waves in the immediate neighborhood of the laser beam. The phase peak increases again due to the enhanced confinement as more of the sideway surface becomes available for thermal-wave interference in the immediate neighborhood of the laser beam, leading to a larger phase lead compared to the flat solid, which can only exhibit interference between front and back surfaces. The normalized phase exhibits broadened width with a decreasing θ_0 due to the increased surface area

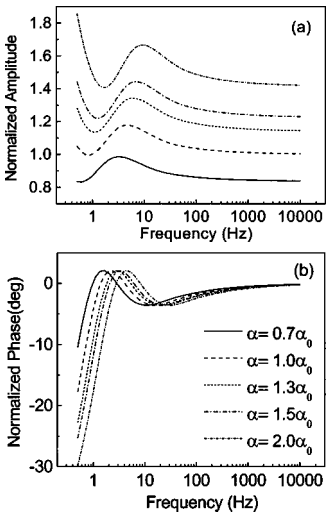

FIG. 5. Effect of thermal diffusivity of the material on the normalized surface thermal-wave amplitude and phase for a cylinder with a 3-mm diameter and measured at $r=R_0$, $\varphi=90°$, and $\theta_0=180°$.

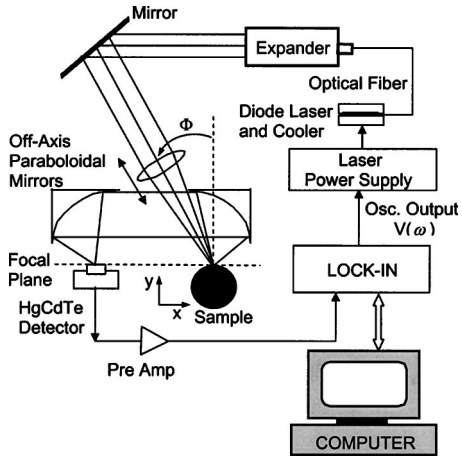

FIG. 6. PTR experimental setup.

contributing to interference. The very shallow phase minimum progressively moves to higher frequencies for the same reason as the amplitude peaks do. The fixed position of the phase maximum, however, is due to the primary interference resulting from the fixed radius of the cylinder, and it corresponds to the slightly frequency-shifted but nearly fixed trough of the amplitude below the peak. The radius-size dependence of these features can be seen in Fig. 1.

Figure 5 shows the effect of the thermal diffusivity of the material on the thermal-wave field measured at $\varphi=90°$ and at an illumination angle $\theta_0=180°$ for a sample with a diameter of 3 mm. As the thermal diffusivity increases, the amplitude increases and the interference becomes more pronounced. This is so because the effects of the presence of the curved boundary become more pronounced and so does the thermal mismatch at the solid-air interface thus trapping more thermal energy within the cylindrical confines. As expected, in both the amplitude and the phase, the peak/valley positions shift toward a higher frequency as the thermal diffusivity increases. Therefore, the peak/valley frequency position of the thermal-wave field provides a unique feature for the determination of the thermal diffusivity of the material once the diameter is known.

IV. EXPERIMENTAL AND DISCUSSION

To verify the foregoing theoretical model, PTR experiments were performed using a series of AISI 1018 cylindrical steel samples. All the samples were machined to a length of 25 mm, and the diameters ranged from 1.5 to 18 mm. The experimental system is shown in Fig. 6. It consisted of a high-power semiconductor laser (~10 W). The output of the laser was modulated by a periodic current, the frequency of which was controlled by the computer and also served as the lock-in reference. The beam was expanded, collimated, and then focused onto the surface of the sample with a spot size ranging from ~1 to 21 mm by adjusting the position of the lens. The harmonically modulated infrared radiation from the sample surface was collected by an off-axis-paraboloidal mirror system and detected by a HgCdTe detector. The signal from the detector was amplified by a low-noise preamplifier and then fed into a lock-in amplifier, which was interfaced with a PC.

The experimental setup was initially optimized using a flat-surface sample, such that both sample and detector were aligned onto the focal plane. This was done using a focused beam because the crossing point of the focused beam with the flat surface matches, most sensitively, the focal point of the paraboloidal mirror system when the beam is focused. When the flat-surface sample was replaced by a cylindrical surface, the thus determined focal plane was the optimized Y position for the cylindrical sample. Scanning the sample along the X direction to maximize the signal determined the optimized X position. By doing so, the top point of the sample (i.e., the point that is tangential to the focal plane) was exactly placed (within reasonable experimental error) at the focal point of the paraboloidal system. Therefore, the detector was monitoring the thermal-wave field emissions from this point. The thermal-radiation information from other points of the sample would not be received by the detector, which is especially true for the curved surface due to the strong defocusing (receding) effect of the curvature. After this procedure, the laser beam was expanded to ~20 mm in diameter by moving the lens such that the laser beam was large enough to conform with the "infinite" z-axis illumination assumed in the model and also to validate the 1D model in the case of a flat sample. It should be noted that the detector always monitored the thermal wave at the focal point of the paraboloidal system (i.e., the tangential point of the sample with the focal plane) because the position of the sample remained unchanged.

Figures 7 and 8 show the experimental results and the corresponding theoretical fits for the two AISI 1018 steel samples (composition: 0.14%–0.2%C, 0.6%–0.9%Mn) with diameters of 1.5 and 3.0 mm, respectively. The fitting was performed using either the amplitude data (Fig. 7) or the phase data (Fig. 8). The corresponding theoretical phase value in Fig. 7 and the amplitude value in Fig. 8 are calculated with the fitted parameters, respectively. Both results show good agreement between the experiments and the theoretical model. The best-fitted thermal diffusivities are

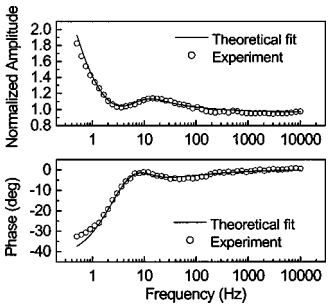

FIG. 7. Fitting results of the amplitude and the phase for a cylindrical steel sample with a diameter of 1.5 mm. The theoretical fits were performed using experimental amplitude data. The theoretical phase value was calculated using the fitted parameters.

13.21×10^{-6} m^2/s and 13.14×10^{-6} m^2/s, respectively from Figs. 7 and 8, which are in excellent agreement with the literature value of 13.57×10^{-6} m^2/s.[15] In the fitting process, we also introduced the measurement angle φ as a fitting parameter to allow us to take into account this experimental factor. The fitted angle results are 56.2° and 55.6° for the 1.5- and 3-mm-diameter samples, respectively, which show good inherent consistency between the two measurements because the laser-beam incidence angle was fixed.

The necessity of introducing the angle factor can be understood from the experimental setup in Fig. 6, in which the laser beam is actually incident onto the cylinder sample at an angle Φ with respect to the normal to the focal plane, as contrasted to the configuration shown in Fig. 1, in which the incident radiation is along the $\varphi=90°$ direction. The detailed orientation of the sample and the incident beam is shown in Fig. 9. As described previously, the thermal-wave field was measured at point *B*, which is the tangential point of the cylinder with the focal plane. Viewing the orientation of Fig. 9, the temperature field that was measured is actually at the $\varphi=90°-\Phi$ angle, with point *A* as a 90-degree reference. In our experiment, the laser beam was approximately incident at an angle of 35°; therefore, the angle φ fit results agree very well with the experimental settings. It should also be noted that the uniqueness of the measured values of the thermal diffusivity and the measurement angle φ extracted from the theoretical fits can be assured due to the totally different dependencies of the thermal-wave field on these two parameters, as witnessed in Figs. 3 and 5, respectively. Especially considering the phase behavior, the peak/valley magnitude

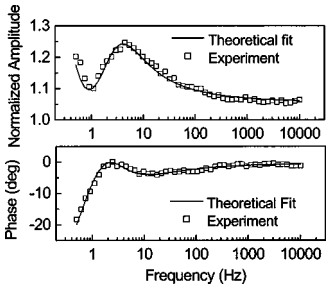

FIG. 8. Fitting results of the amplitude and the phase for a cylindrical steel sample with a diameter of 3.0 mm. The theoretical fits were performed using the experimental phase data, and the theoretical amplitude value was calculated using the fitted parameters.

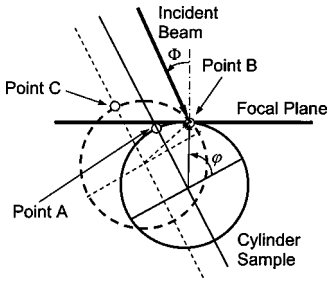

FIG. 9. Details of the geometrical orientation of the sample and the incident laser beam.

difference remains unchanged when the thermal diffusivity changes, whereas the same difference changes significantly with the measurement angle. This fact is of great interest in practice because it assures that one does not have to measure the actual incidence angle of the laser beam in order to obtain the thermal diffusivity. Also indicated in Fig. 9, the dashed cylindrical cross section shows another position of the sample in the experimental system, for which the measurement point *B* is located at a large incidence angle (small φ in the equation) with respect to the 90°-reference point *C*. This dashed cylindrical position shows how to measure the thermal-wave field at different angles on the sample surface, which can be implemented in two steps: by moving the cylinder along the *X* direction first and then along the *Y* direction, such that the desired measurement point on the surface is coincident with the focal point.

V. CONCLUSIONS

We have formulated a new thermal-wave model that is suitable for characterizing cylindrical samples using photothermal radiometry. Based on the Green function method, the thermal-wave field from a cross section of an infinite-height cylinder was obtained. It was found that the thermal diffusivity of the material is the only thermophysical property involved in the frequency dependence of the thermal-wave field. The thermal-wave-profile dependencies on various thermophysical and geometrical parameters were discussed. The theoretical model was further validated by suitable experiments, in which cylindrical steel samples with different diameters were measured and compared with literature values. This work offers a PTR technique for characterizing cylindrical samples without the requirement of flat surfaces, as in the conventional PTR method. It is thus expected that the present methodology can be applied to the quantitative thermophysical characterization of thin wires, screws, and other industrial types of metallic rods.

ACKNOWLEDGMENT

The support of Materials and Manufacturing Ontario (MMO) is gratefully acknowledged.

[1]P. E. Nordal and S. O. Kanstad, Phys. Scr. **5–6**, 659 (1979).
[2]R. D. Tom, E. P. O'Hara, and D. Benin, J. Appl. Phys. **53**, 5392 (1982).
[3]R. Santos and L. C. M. Miranda, J. Appl. Phys. **52**, 4194 (1981).
[4]L. Fabbri and P. Fenici, Rev. Sci. Instrum. **66**, 3593 (1995).
[5]L. Qian and P. Z. Li, Chin. Phys. **11**, 417 (1991).
[6]A. Ocariz, A. Sanchez-Lavega, and A. Salazar, J. Appl. Phys. **81**, 7552

(1997).
[7]F. Garrido and A. Salazar, J. Appl. Phys. **95**, 140 (2004).
[8]A. Salazar, A. Sanchez-Lavega, and R. Celorrio, J. Appl. Phys. **93**, 4536 (2003).
[9]T. Borca-Tasciuc and G. Chen, Rev. Sci. Instrum. **68**, 4080 (1997).
[10]A. Mandelis, *Diffusion-Wave Fields: Mathematical Methods and Green Functions* (Springer, New York, 2001), Chaps. 2.3, 2.9 and 6.19.
[11]J. V. Beck, K. D. Cole, A. Haji-Sheikh, and B. Litkouhi, *Heat Conduction Using Green's Functions* (Hemisphere Publishing Corporation, Washington, DC, 1992), p. 11.
[12]H. S. Carslaw and J. C. Jaeger, *Conduction of Heat in Solids* (Oxford University Press, Oxford, 1959), pp. 20 and 263.
[13]G. C. M. Meijer and A. W. Herwaarden, *Thermal Sensors* (Institute of Physics Publishing, Bristol, 1994), pp. 1–22.
[14]*Handbook of Mathematical Functions*, Applied Math Series 55, edited by M. Abramowitz and I. A. Stegun (National Bureau of Standard, Washington DC, 1964).
[15]Metals Handbook, 10th ed. (ASM International, Material Park, Ohio, 1990), Vol. 1, p. 196.
[16]A. Mandelis, L. Nicolaides, and Y. Chen, Phys. Rev. Lett. **87**, 020801 (2001).
[17]C. A. Bennett and R. R. Patty, Appl. Opt. **21**, 49 (1982).
[18]J. Shen and A. Mandelis, Rev. Sci. Instrum. **66**, 4999 (1995).